Chapter 12

Synthesis of $Ba_{1-x}Ca_xTiO_3$ by Complex Polymerization Method (CPM)

Fabiana V. Motta, Ana Paula A. Marques, Carlos A. Paskocimas, Mauricio R. D. Bomio, Amélia S. F. Santos, Edson R. Leite, José A. Varela and Elson Longo

Additional information is available at the end of the chapter

http://dx.doi.org/10.5772/46015

1. Introduction

Oxide powders have been synthesized by solid-state reaction, using binary oxides or carbonates as precursors have been reported. The reaction with necessity of high temperatures and longer reaction times are obstacles in materials synthesis process because of yours high cost and because the use of high temperatures [1,2].

In the Complex Polymerization Method (CPM) theses problems are reduced because the synthesis occurs at low temperature and reduced reaction times are required, and, the immobilization of the metal complexes in such rigid organic polymeric networks can reduce the metal segregation, thus ensuring the compositional homogeneity at the molecular scale [3].

Organic polymer precursors are often utilized in the synthesis of multicomponent oxide powders. In the Pechini process, an aqueous solution of ethylene glycol, citric acid, and metals ions is polymerized to form a polyester resin. The compositional homogeneity is of vital importance for the synthesis of multicomponent oxides with complicated compositions, since the chemical homogeneity, with respect to the cation distribution throughout the entire gel system, often determines the compositional homogeneity of the final multicomponent oxides [4]. This method has been used to synthesize nanoparticles and thin films of several ferroelectric materials. The development of new semiconductor materials with wide band gaps (2.0–4.0 eV) may give rise to newoptoelectronic devices, particularly to materials for application in the development of green or blue light emission diodes (LED) or laser diodes. In many optoelectronic devices, amorphous semiconductors can replace single crystal semiconductors, particularly when cost is an important factor [5].

The CPM achieves molecular mixing of the starting materials and has been successfully used to synthesize several compounds, including $BaTiO_3$, $Pb(Zr,Ti)O_3$ and $BaMoO_4$ [6-10]. The barium titanate ($BaTiO_3$) perovskite, that is one ferroelectrics material, have been extensively studied due several possible applications such as electronic and optical devices [11-15]. The substitution of Ba by Ca in the $BaTiO_3$ perovskite results in an improvement of the stability of the piezoelectric properties, consequently the barium calcium titanate ($Ba_{1-x}Ca_xTiO_3$) solid solution has attracted great attention for use in the laser systems, eletro-optic material for various photorefractive and holographic applications [16-18]. The production of Ca-doped $BaTiO_3$ compounds by solid state reaction method the mixture of $BaCO_3$, $CaCO_3$ and TiO_2 is heat treated at high temperatures for long times and requires two successive calcinations to get high solubility of Ca^{2+} in the $BaTiO_3$ matrix [19-21]. It has been observed that Ca^{2+} replaces Ba^{2+} in $Ba_{1-x}Ca_xTiO_3$ to form tetragonal BCT solid solutions when x is less than ~0.23 [22, 23]. Moreover, Cheng et al. [23] obtained pure tetragonal phase for $x \leq 0.25$ and mixture of phases for x in the range of 0.3-0.85.

Photoluminescence (PL) property at room temperature occurs due to structural disorder existing in the perovskite system [24, 25]. However, the system can not be fully disordered owing to present a minimal order in the structure. This means that there is an order-disorder rate which favors the PL phenomenon in the system. Disorder in materials can be manifested in many ways: some examples are vibrational, spin and orientation disorder (all corresponding to a periodic lattice) and topological disorder. We will concentrate principally on the latter, which is the type of disorder associated with the structure of glassy and amorphous solids, a structure that cannot be defined in terms of a periodic lattice. Photoluminescence (PL) is a powerful probe of certain aspects of short-range order in the range of 2–5 Å and medium range of 5–20 Å, such as clusters, where the degree of local order is such that structurally inequitable sites can be distinguished because of their different types of electronic transitions and are linked to a specific structural arrangement [26]. The order was related to the presence of $[TiO_6]$ clusters, whereas the disorder was related to the presence of $[TiO_5]$ clusters. It is believed that PL occurs due to interaction of TiO_5-TiO_6 [27]. This PL emission was attributed to localized levels above the valence band (VB) and below the conduction band (CB). It has been demonstrated that a series of structurally disorder titanates synthesized by a soft chemical process have shown intense photoluminescence (PL) at room temperature [28-30]. In such cases, a minimal order in the system is necessary for the material exhibit PL property at room temperature.

Considering that the CPM is efficient to promote produce structural order-disorder complexes oxides powders and few have has been reported about the property PL of the barium calcium titanate (BCT). In this chapter, we present a detailed the synthesis and the effect structural of Ca^{2+} in the $BaTiO_3$ matrix powders of the conditions that favor the PL emission at room temperature.

2. Experimental section

2.1. Materials

The starting chemicals included titanium (IV) isopropoxide [$Ti[OCH(CH_3)_2]_4$ (Aldrich 97%), citric acid ($H_3C_6H_5O_7$) (Merck 99.5%), $CaCO_3$ (Aldrich 99 +%), $BaCO_3$ (Aldrich 99 +%), NH_4OH (Merck 99%) and ethylene glycol ($HOCH_2CH_2OH$) (J. T. Baker 99%). All of the chemicals were used without further purification.

2.2. Synthesis

$Ba_{1-x}Ca_xTiO_3$ (x = 20 % mol) was prepared by the Complex Polymerization Method (CPM) using barium carbonate ($BaCO_3$), calcium carbonate ($CaCO_3$) and titanium (IV) isopropoxide [$Ti[OCH(CH_3)_2]_4$ as starting materials. A flow chart representing of the synthesis by the CPM of BCT20 is outlined in Figure. 1. In this synthesis, the titanium citrate (TC) was formed by dissolution of titanium (IV) isopropoxide in aqueous solutions of citric acid (CA). The molar ratio of (CA) to titanium (IV) isopropoxide was 4:1. The citrate solution was well homogenized under constant stirring at a temperature of ~ 60-70°C, pH ~ 1.5. After achieving complete dissolution was add stoichiometric amounts of barium carbonate and calcium. The complex was well stirred for several hours at 60–70°C to produce a clear, homogeneous solution. After the solution was homogenized, ethylene glycol was added to promote the polyesterification. The citric acid/ethylene glycol mass ratio was set at 60:40. With continued heating at 100–120°C, the viscosity of the solution increased, albeit devoid or any visible phase separation. After partial evaporation of the water, the resin was heat

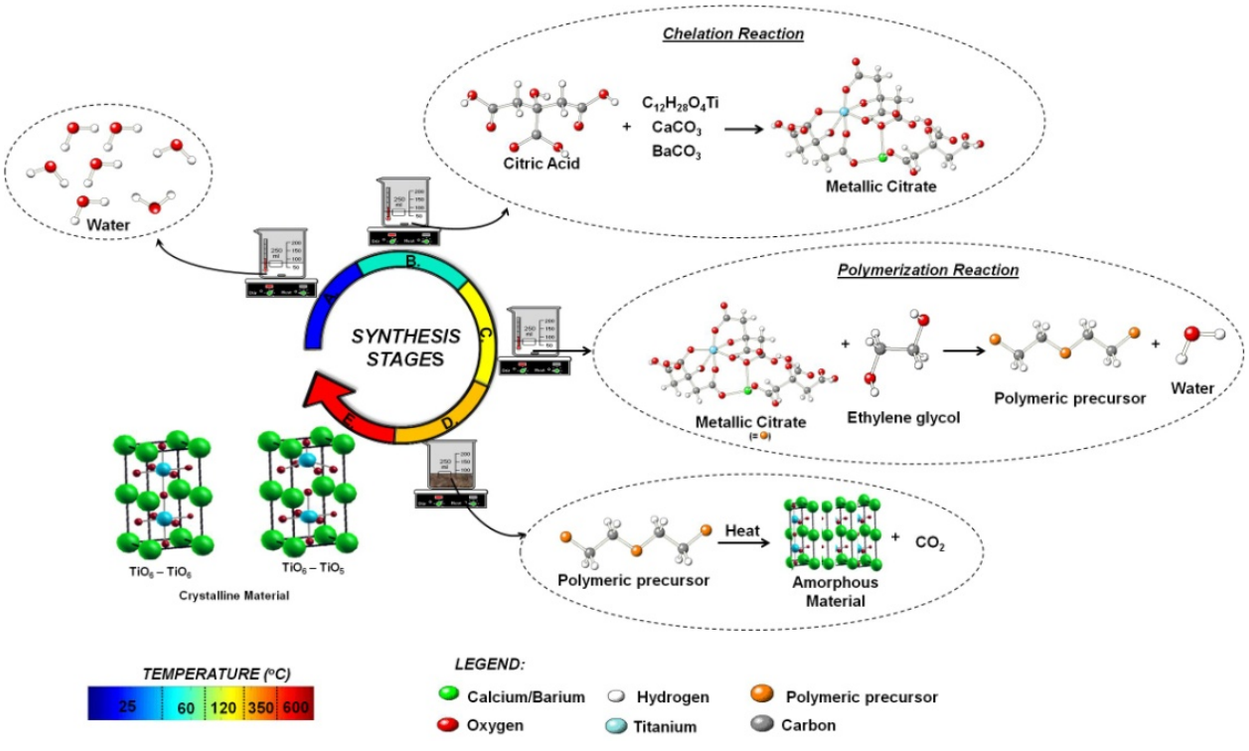

Figure 1. Flowchart representing the procedure for the synthesis of BCT20 powders.

treated at 350°C for 2 h, in a static oxidizing atmosphere, leading to the partial decomposition of the polymeric gel, forming an expanded resin, constituted of partially pyrolyzed material. This pre-pyrolyzed material (dark-brown powders) was removed from the beaker and deagglomerated using mortar. The powders were annealed at 400, 450, 500, 550, 575 and 600°C for 2 h.

2.3. Characterizations

FTIR transmittance spectroscopy and Liquid-state ^{13}C NMR at room temperature were performed on chemical solutions of TC (Ti-CA) and BCT (Ti-CA-Ba-Ca) at the initial reaction stage, before the polyesterification reaction by (EG). This study was carried out in order to compare the structures of complex species in these initial phase. The ^{13}C NMR characterization was conducted with a ^{13}C resonance at room temperature on a Bruker DRX 100Mz, 9.4T. These initial solutions and the calcined powder of BCT compounds (400°C ≤ T ≤ 900°C) were characterized by Fourier transformed infrared (FTIR) spectroscopy. The FTIR transmittance spectra were taken in the frequency range of 400–4000 cm^{-1} using an Equinox/55 (Bruker) spectrometer after disk samples was formed with KBr.

The thermal properties of the calcined dark-brown powders were investigated by simultaneous thermogravimetric analysis (DTA and TG) using a TA Instruments machine under oxygen flow (100 cm^3/min) and subjected to heating rate of 5°C/min at room temperature (~ 20°C) to 900°C. Samples were placed in platinum crucibles, weighing typically 8 mg, and a calcined alumina crucible was used as the reference material.

Powder X-ray Diffraction (XRD) patterns were collected from the heat-treated samples using a Rigaku diffractometer, model D/max-2500/PC with Cu Kα radiation. The X-ray diffraction data for the 1200°C sample were analyzed by the Rietveld method as implicated in the FULLPROF program, taking tetragonal perovskite (*P*4*mm*) as the starting model. A pseudo-Voigt function was fitted by refinement of the scale factor, background, peak width, peak asymmetry, atomic positions and lattice constants.

The Raman spectra for powders were obtained at room temperature using a RFS/100/S Bruker FT-Raman equipment over the scan range of 100-1400 cm^{-1}, using the 1064 nm exciting wavelength of a Nd:YAG laser. The infrared (IR) spectra were taken to characterize the lattice vibration of powders calcined at the different temperatures.

The PL spectra were collected with a digital monochromator internally integrated to a CCD with optical resolution of 1 nm and accuracy of 0.1 nm (Newport, OSM-400UV/VIS-U), using a time integration of 4 s (2.9 x 10-17 W per count/s) coupled to a optical fiber. The 355 nm exciting wavelength of a third harmonic of a Nd:YAG Q-switched laser (Brilliant B from Quantel) with a pulse duration of 4 ns and a repetition rate of 10 Hz was used, with an average energy of 4 mJ per pulse. The 488 nm exciting wavelength of a tunable optical parametric oscillator (OPO) pumped by 355 nm (3W) of a Q-switched Nd-YAG laser was also used, with an average energy of 4 mJ per pulse. All the measurements were taken at room temperature.

3. Results and discussion

3.1. Characterization of the precursor solution

CA-metal chelation in the precursor was accompanied by IR and NMR spectroscopy, in order to analyze the barium-calcium-titanium-citric acid complexes. Figure 2 shows the FTIR absorption spectra of TC and precursor solution of BCT. In the pH range 1–2, two peaks of asymmetric carboxyl groups are evident for the Ti-CA resin (TC) spectra; one at 1724 and the other at 1635 cm^{-1} referent to $\upsilon_{as}(COOH)$ and $\upsilon_{as}(COO^-)$, respectively. Symmetric stretching frequencies occurred at 1445 and 1389 cm^{-1} for the same carboxyl groups [31, 32]. BCT resin spectra do not display a unionized carboxyl group in the region close to 1720 cm^{-1}, indicating that all carboxyl groups were ionized in ph ~8.5 [33]. In the BCT spectra, two bands belonging to asymmetric and symmetric stretching are attributed, according to Rajendran et al. [31] and Yasodhai et al. [32], to the presence of a mixed-metal CA complex in BCT, which creates different types of carboxyl groups. In all complexes, the carbonyl asymmetric and symmetric stretching frequencies were in the range of 1665-1565 cm^{-1} and 1445-1389 cm^{-1}, respectively. The difference between the asymmetric (ν_{as}) and symmetric (ν_s) COO stretching modes ($\triangle(\nu_{as}-\nu_s)$) of the coordinated carboxyl groups varied from 220 to 176 cm^{-1}, suggesting that the carboxyl groups present an unidentate coordination in these resins [31, 32]. If the carboxyl groups were involved in bridging in the chelation of CA complex, the value for $\triangle\nu$ would be expected to be lower than $\triangle(\nu_{as}-\nu_s)$ ~ 170 cm^{-1} [32]. In the region below 1000 cm^{-1} a broad band that was attributed to stretching of the bond M-O appears, where M is Ti, Ba or Ca [34]. Similar bonds were verified by 13C NMR measurements performed on this solution, as discussed below.

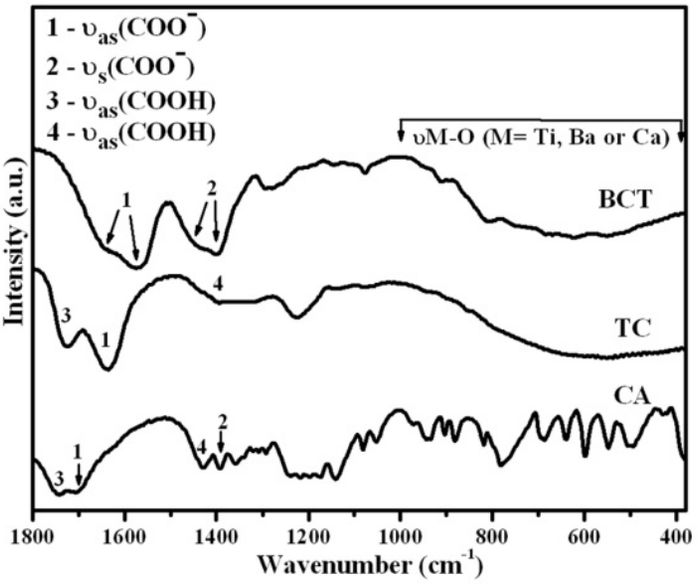

Figure 2. FTIR absorption spectra of free citric acid (CA), titanium citrate (TC), and precursor resin (BCT).

Figure 3(a) illustrates the ^{13}C NMR spectra for the Ti-CA solution with pH value close to 1.5. This figure revealed the presence of eight resonance signals, which were assigned to the free

CA and Ti-CA complex. The free CA is characterized by the four typical signals at 45.5, 75.5, 175.6, and 178.9 ppm. These four peaks represent the carbon centers in the methylene groups (CH_2 – C2 and C3 carbons), the alcoholic groups (COH – C1), the terminal carboxylic acid groups (t-COOH – C4 and C5), and the middle carboxylic acid groups (m-COOH – C6) of free CA, respectively [4, 33]. The other four signals are weak and the broad absorption signal is compared to the same peak of the free CA, this is a characteristic of coordination compounds with transition metals. The binding of Ti with CA can occur at different points of the CA chain, -COH, -mCOOH and -tCOOH. As the Ti ion is electron deficient, it can promote dislocations of the electronic density, possibly causing strengthening in bindings near Ti (C1′, C5′ and C6′). The resonance signal referent to C1′, C5′ and C6′ are 90.4, 175.9 and 187.8 ppm, respectively [4, 33]. The shifts of the alcoholic groups (Δδ 14.9 ppm) at 75.5 ppm and the middle carboxylic acid group (Δδ 8.9 ppm) at 178.9 ppm indicate that the –COH and –mCOOH groups in citric acid simultaneously coordinate the titanium atom. A small shift (Δδ 0.3 ppm) is observed for the uncoordinated –tCOOH, according to Deng et al. [35]. The resonance signal of the C2′, C3′ and C4′ in Ti-CA complex is not affected, consequently resonance signals of these carbons with the metals are similar to the free CA. Figure 3(b) shows a typical ^{13}C NMR spectrum of BCT solution, with the pH value at around 8.5. This figure revealed that all resonance signals belonging to BCT appear in larger ppm values (deshielding) than Ti-CA. This is related to the pH value of the BCT and Ti-CA solutions that are close to 8.5 and 1.5, respectively. Higher pH values (8-9) promote the deprotonation of the CA, in which the carbons of the acid groups are strongly linked with oxygen and come back more unprotected, the outcome is that more energy is necessary to make these carbon resonates and resonance signals to be shifted to larger ppm values (unshielded) compared to the systems with lower pH values [33]. The -tCOOH carbon group exhibits signals at around 180.9 and 180 ppm for Ba-C5″ and Ti-C5″, respectively [4, 33]. Resonance signals at around 77.7, 86.4, 91.5, 183.9, 189.3 and 190.3 belong to COH (C1), -COHBa (C1′′), -COHTi (C1′), -mCOOH (C6), -mCOOBa (C6′′) and -mCOOTi (C6′), respectively [4, 33]. The 13C NMR spectra of BCT resembled that of Ti-CA complex. Large downfield of the –COH (Δδ 8.7 and 13.8 ppm) and -mCOOH (Δδ 5.4 and 6.4 ppm) carbons groups related to the free citrate are observed for the complexation of CA with Ba^{2+} and Ti^{4+}, respectively [35]. The resonance signal around 47.8 ppm is attributed to the carbon center in the methylene groups (CH_2 – C2 and C3 for the free CA and C3 for the BCT). The resonance signal of the carbon center C2 in BCT is close to 47.1 ppm [4, 33].

3.2. Characterization of the calcined powders (BCT20)

The thermal decomposition of the pre-pyrolyzed (300°C for 2 h) BCT sample in synthetic air atmosphere is shown in Figure 4. The thermogravimetric analysis (TGA curve) shows four decomposition stages. First, TGA indicated a weight loss of ~ 15 % in the range of 25-120°C, which is related to the elimination of water and ethylene glycol. Second, it denoted a weight loss of ~ 62 %, as can be observed in the temperature range of 120 to 480°C, which is probably related to the decomposition of polymeric chains and the elimination of CO_2 and H_2O. A third weight loss of ~ 5 % occurs in the temperature range of 480-558°C and is

attributed to the formation of $(Ba_{0.8}Ca_{0.2})_2Ti_2O_5.CO_3$ [36]. Lastly, from 558-675°C onward, the decomposition of intermediate phases occurs with a ~ 3 % weight loss during crystallization of pure BCT20 as the final reaction product. Above 675°C, no obvious weight loss was observed. Kumar and Messing [36] reported that the following two-stage process could represent such transformation.

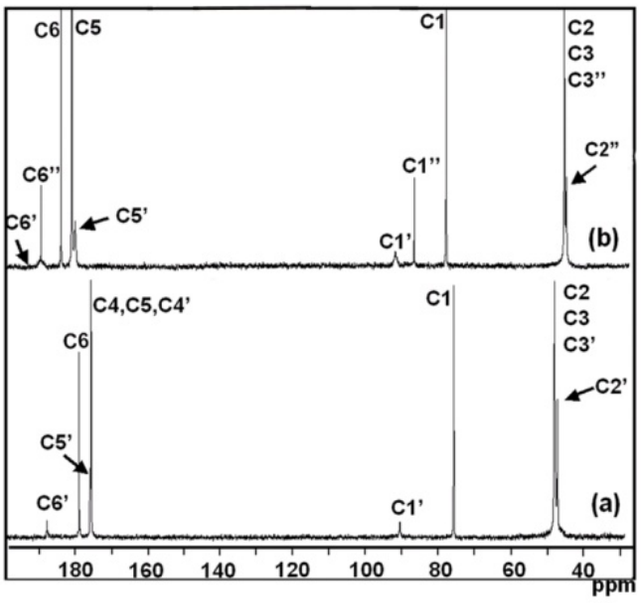

Figure 3. ^{13}C NMR spectra of: Ti-CA solution with pH ~1.5 (a); and BCT solution with pH ~ 8.5 (b). Here C = carbon centers in a citric acid free; C′ = carbon centers in a citric acid affected by Ti, and C′′ = carbon centers in a citric acid affected by Ba.

$$\text{Ba, Ca, Ti precursor}_{(s)} + \text{air}_{(g)} \rightarrow \text{Ba, Ca,Ti oxycarbonate}_{(s)} + CO_{2(g)} \quad (1)$$

$$\text{Ba, Ca, Ti oxycarbonate}_{(s)} \rightarrow 2\ Ba_{0.8}Ca_{0.2}TiO_{3(s)} + CO_{2(g)} \quad (2)$$

DTA revealed the presence of a peak at temperatures close to 450 °C (Figure 4). This exothermic peak is assigned to organic species pyrolysis, during rupture of the polymeric chain. The low loss mass of the TG/DTA curves above T ~ 500°C suggests the beginning of the crystallization process. Moreover, it is important to notice the presence of two low intense exothermic peaks at 520 and 650 °C, which could indicate the formation and decomposition of intermediate phases as, for example, complex Ba, Ca and Ti carbonates.

Figure 5 shows the XRD patterns of the BCT20 powders heat treated at different temperatures, from 400 to 600°C. In this figure it is observed that the BCT20 heat treated at 400°C is disordered. This result is in agreement with the previous TG/DTA analysis and with those described in literature, indicating that the crystallization process occurs at temperatures higher than 450°C. The materials heat treated between 450-550ºC present only broad diffraction reflections at 2θ ~ 24.3°, 26.7º and 34.7º referent to the barium titanium oxycarbonate, $(Ba_{0.8}Ca_{0.2})_2Ti_2O_5.CO_3$ [37].

The X-ray patterns of heat-treated samples at 575°C display the Bragg reflections of this intermediate phase and two peaks at 2θ ~ 22º and 31.6º, which can be indexed as being characteristic of the perovskite BCT phase.

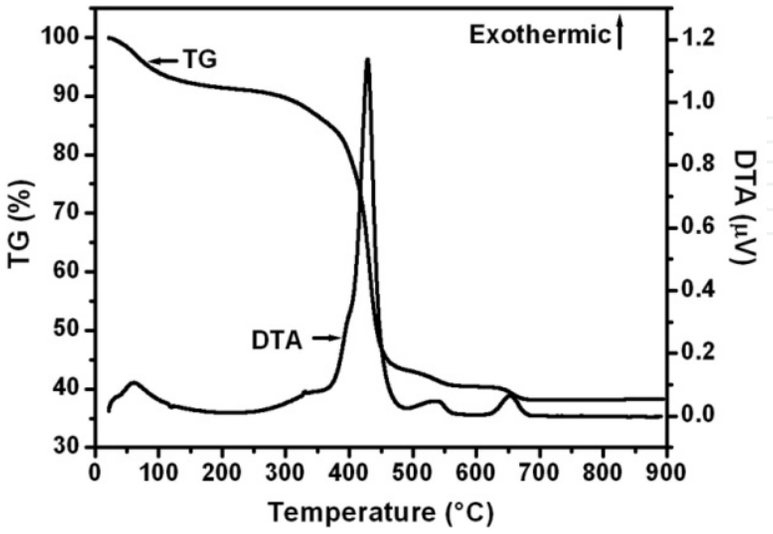

Figure 4. TGA/DTA range 25 - 900°C in synthetic air atmosphere of BCT pre-pyrolyzed at 300°C for 2 h.

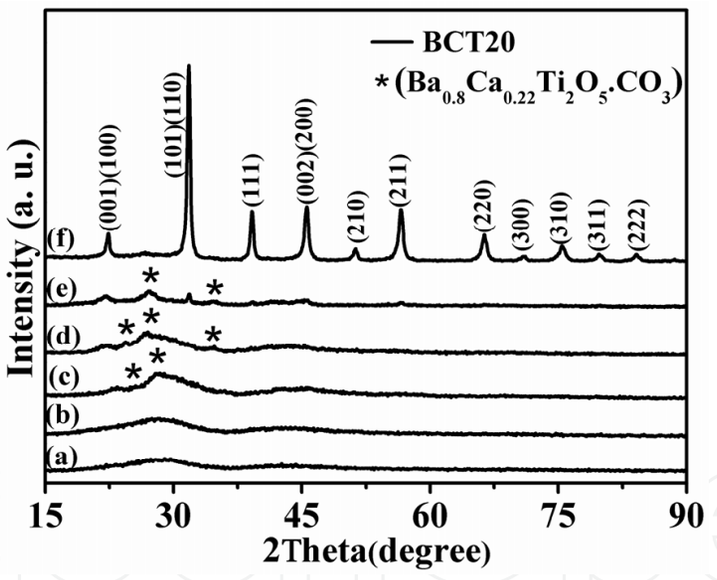

Figure 5. XRD patterns of the BCT powders calcined at temperatures: (a) 400°C; (b) 450°C; (c) 500°C; (d) 550°C; (e) 575°C and (f) 600°C.

The crystallization and decomposition process of this intermediate phase can be related to the presence of both exothermic peaks in the DTA curve. All samples heat-treated at 600°C are single-phased, with all Bragg reflections belonging to the perovskite BCT20. The pure BaTiO3 (BT) ceramic shows a tetragonal phase as identified and indexed using the standard XRD data of the corresponding BCT20 powders [19, 22]. The lattice parameters and the mean crystallite sizes were calculated from the peak positions displayed in Figure 5. The ordered BCT20 calculated crystallite sizes were around of 17 nm. The lattice parameters *a*

and *c* were obtained using the least square refinement from the REDE93 program. The lattice parameters a and c were around of 3.9607(3) Å and 3.9941(3) Å, respectively; similar to the values reported for $Ba_{0.773}Ca_{0.227}TiO_3$ crystals (a = 3.962 Å and c = 3.999 (Å) [22]. The absence of the CT phase in the X-ray patterns of the BCT powders also suggests that samples prepared by this method present effective complexation of the Ca^{2+} ions in the matrix of $BaTiO_3$.

The Figure 6 depicts spontaneous Raman spectra of BCT20 powders recorded at the room temperature for samples calcined from 400-600°C. The samples heat treated at 400 and 450°C no present well-resolved sharp peaks in the Raman spectra, indicating that the material is structurally disordered at short range. The Raman spectra of powders heat treated between 500 and 575°C exhibited a fluorescent-like background. The band around of 1061 cm^{-1} (marked with a • in Figure 6) were attributed to the $(Ba_{0.8}Ca_{0.2})_2Ti_2O_5.CO_3$ intermediate phase [34]. Bands of the intermediate phase disappear completely in the powders heat treated at 600°C, agreeing with XRD data. These alterations were accompanied by appearance of five distinct broad bands referent to the $BaTiO_3$ *P*4*mm* tetragonal phase: 726, 526, 304, 256 and 186 cm^{-1} with its respective vibration modes $A_1(LO_3)$, $A_1(TO_3)$, E(TO), $A_1(TO_2$ and $A_1(TO_1)$ (marked with a ❖ in Figure 6) [2, 34]. The Raman peaks at 153 and 640 cm^{-1} (marked with a ◊ in Figure 6) were attributed to the satellite peaks, according to Cho et al. [2], however these peaks can be attributed too the $BaTiO_3$ hexagonal phase.

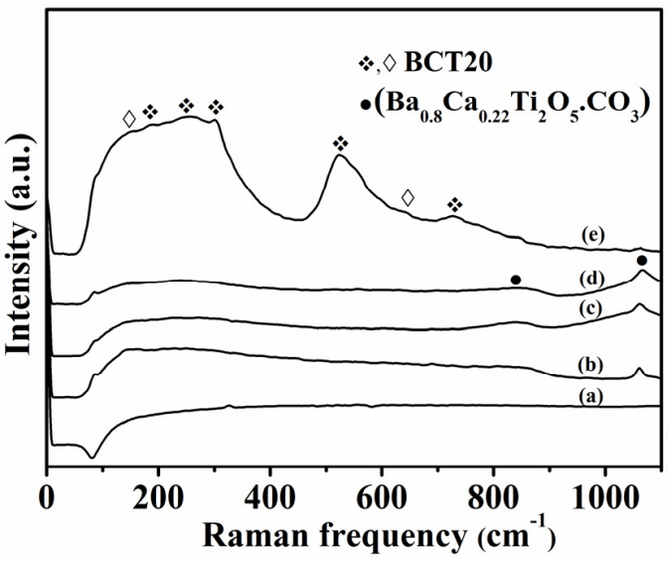

Figure 6. Spontaneous Raman spectra of BCT20 powders heat treated at (a) 400°C, (b) 500°C, (c) 550°C, (d) 575°C and (e) 600°C

The morphology of the BCT20 powders was investigated using HR-SEM. Figure 7 presents micrograph of powders heat treated at (a) 500°C and (b) 600°C. The powders calcined in the 400 - 575°C range for 2 h show free particles agglomerate with irregularly shaped Figure 7(a). The Figure 7(b) shows an agglomerate grain growth into of individual particles with irregularly forms developed as a result of the massive organic burn-off and consequent gas evolution, these characteristic were analogous to the powders treated at 600°C.

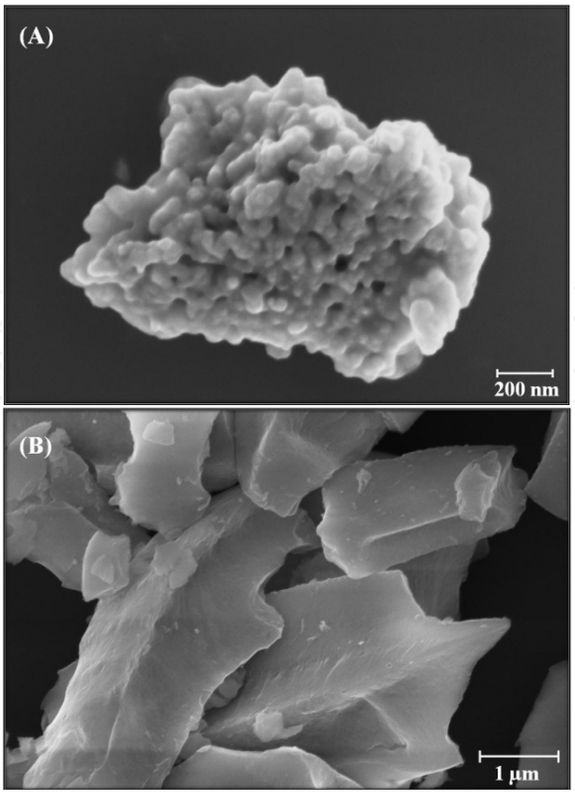

Figure 7. HR-SEM micrograph of BCT20 powders heat treated at (A) 500 °C and (B) 600 °C for 2 h.

Additional structural characterization was performed by infrared spectroscopy on the BCT20 sample. Figure 8 shows the FTIR spectra of the BCT20 treated at 400-600°C. From the spectrum of BCT annealed at 400-575°C, it is clear that undecomposed organic ligands are still present in the powders, both display a band at 1758 cm^{-1} attributed to C=O stretching mode [34, 38]. The broad absorption band corresponding to the O-H stretching modes in crystallization water occurs close to 3448 cm^{-1} to the BCT. The disordered compounds treated at 400-575°C showed a peak at ~ 1385 cm^{-1}, which was associated to the carboxylate group stretching mode [34, 38]. The spectra of compound heat-treated at 400-575°C present peaks at around 1060, 863, and 690 cm^{-1} that were attributed to carbonate ions ($BaCO_3$) [34]. These peaks seem to have lower intensity as the temperature increases, and in compounds treated at 600°C these peaks are absent. The band related to the carbonate ions were clearly observed for heat treatment up to 575°C (band at around 1450 cm^{-1}) reducing at higher temperatures and almost disappearing at 600°C [34]. In the BCT treated at 500 to 575°C, the peak related to the antisymmetric COO^- stretching mode of unidentate complex is observed at 1631 cm^{-1}, although for the samples heated treated at over 575°C, this peak is absent [34, 38]. The spectrum of the BCT heat-treated at 575-600°C, displays a very broad absorption band at around 522 cm^{-1}, referent to $F_2(\nu_3)$ antisymmetric stretch vibrations, ascribed to the Ti–O stretching vibration in $BaTiO_3$, as reported in literature [34, 38]. By increasing the heat treatment temperature, the crystalline structure seems to be more ordered and the band attributed to the Ti-O bonds, which are more defined. Also, the band at 2350 cm^{-1} refers to the adsorbed CO_2 from atmosphere [8, 9]. Such features are in good agreement with XRD

and Raman Spectroscopy data and also indicate that CPM is effective in the synthesis of BCT powders.

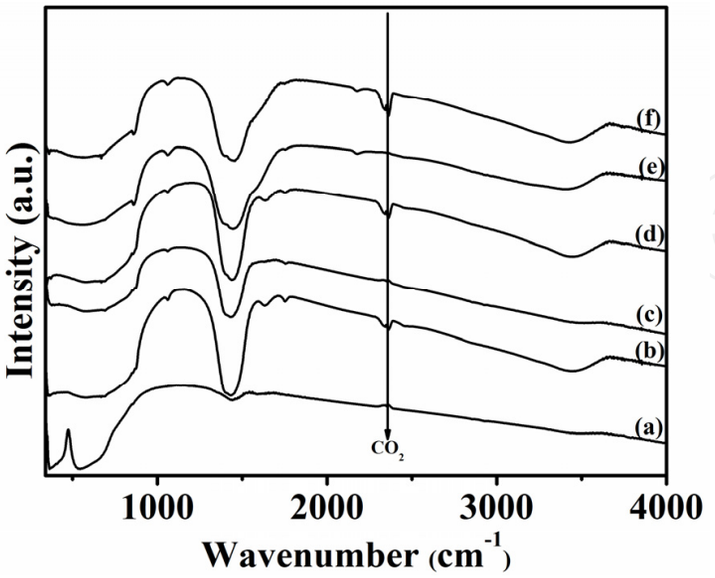

Figure 8. FTIR absorption spectra of dehydrated BCT powders heat treated at (a) 400°C, (b) 450°C (c) 500°C, (d) 550°C, (e) 575°C and (f) 600°C

The photoluminescence spectra recorded at room temperature for BCT20 powders heat treated at 400-600°C in two different excitation wavelength: the 355 nm (Figure 9a) and 488 nm (Fig. 9b) of an Nd:YAG laser system. BCT20 heat treated at 400-575°C presented PL emission. The BCT20 powder annealed at 500°C displays the most significant PL intensity when excited with these two wavelengths laser beam. The system has a totally ordered structure (samples annealed at 600°C), the PL emission is not observed.

This profile of the emission band is typical of a multiphonon process, i.e. a system in which relaxation occurs by several paths, involving the participation of numerous states within the band gap of the material [27]. This behavior is related to the structural disorder of BCT20 and indicates the presence of additional electronic levels in the forbidden band gap of the material.

The complex PL band spectra may be due to several components and generally can be decomposed in individual components. The spectrum is decomposed based on the nature of the process governing each component. The luminescence process is generally described by a Gaussian line broadening mechanism in which case, the luminescence intensity can be expressed in terms of a Gaussian (amplitude version) line-shape function and can be written by the following equation:

$$\mathrm{I}(h\nu) = \mathrm{I}_0 + \sum_{i=1}^{n} A_i \exp\left[-\frac{(h\nu) - E_{0i}}{2\sigma_i^2}\right] \tag{3}$$

where $h\nu$ is the energy of the radiation emitted, I_0 is the offset intensity, A_i is the amplitude of each component, E_{0i} is the energy of each component in which the intensity is maximum, and σ_i is the standard derivation for each component (FWHM) [39].

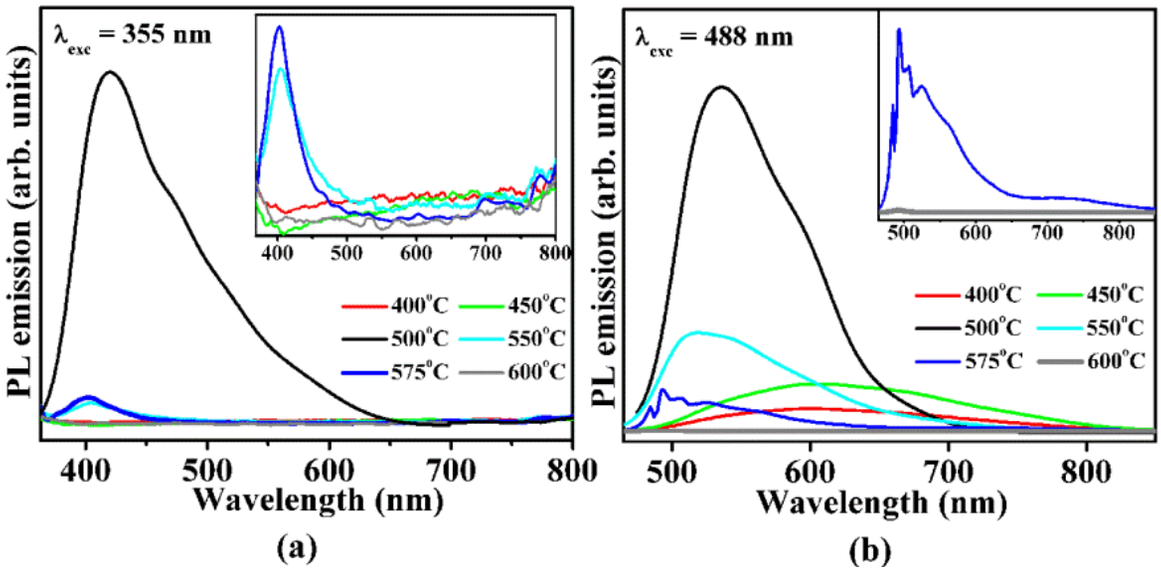

Figure 9. Room-temperature photoluminescence spectra of BCT powder samples annealed at 400, 450, 500, 550, 575 and 600oC for 2 h in an oxygen flow: (a) excitation with 355 nm wavelength of an Nd:YAG laser and (b) excitation with 488 nm wavelength of an Nd:YAG laser

The BCT20 powder annealed at 500ºC displays the most significant PL intensity when excited with these two laser beam wavelengths. Using the Gaussian method, the PL curves of the BCT20 sample annealed at 500ºC were decomposed into components, each of which refers to the region in the visible spectrum where its maximum peak intensity appears. Each color represents a different type of electronic transition and can be linked to a specific structural arrangement. To gain a better understanding of the properties of PL and its dependence on the structural order-disorder of the lattice, the PL curves were analyzed using the PeakFit deconvolution program [40]. Based on the Gaussian line broadening mechanism for luminescence processes, the fine features in the PL spectra of samples annealed at 500ºC were deconvoluted and extracted from the deconvolution curves. Figure 10a and 10b illustrates such decompositions, while Table 1 lists the areas under the curve of the respective transitions.

The decomposition band indicated the presence of different intermediate levels in the band gap. More energetic excitation wavelengths favor the transition of more energetic levels in the band gap. Thus, broad band PL emission consists of the sum of individual emissions. Such emissions arise from a radiative recombination between electrons and holes trapped in the gap states. The transitions of disordered titanates therefore occur at energies far below the band gap of these materials. The violet component is associated with more energetic transitions and is observed only after excitation with a laser beam wavelength of 355 nm. Otherwise, the green component is associated with a less energetic transition and is observed after excitation with a laser beam wavelength of 488 nm [16, 26].

In the structure perovskite-type the lattice former titanium is at the center of the cube, surrounded by six oxygens that occupy the middle of the faces, in a regular octahedral configuration. However, the structure before of get its ideal configuration (totally ordered)

is a mixture of TiO5-TiO6 clusters intercalated by Ba and Ca atoms. The higher the heat treatment temperature, the more frequent the TiO6 conformation and the more ordered the structure [10, 41]. According XRD results the BCT20 powders are ordered annealed at 600°C. The ordered powders where only TiO_6 clusters tend to exist does not allow the creation of point defects and do not presents PL emission at room temperature [10]. Similar to the CT:Sm studied by de Figueiredo et al. [10], the compound with intermediary range disorder (500°C) presented intense PL emission while compared to the compound disordered (400 and 450°C) and the ordered compound no PL property was showed.

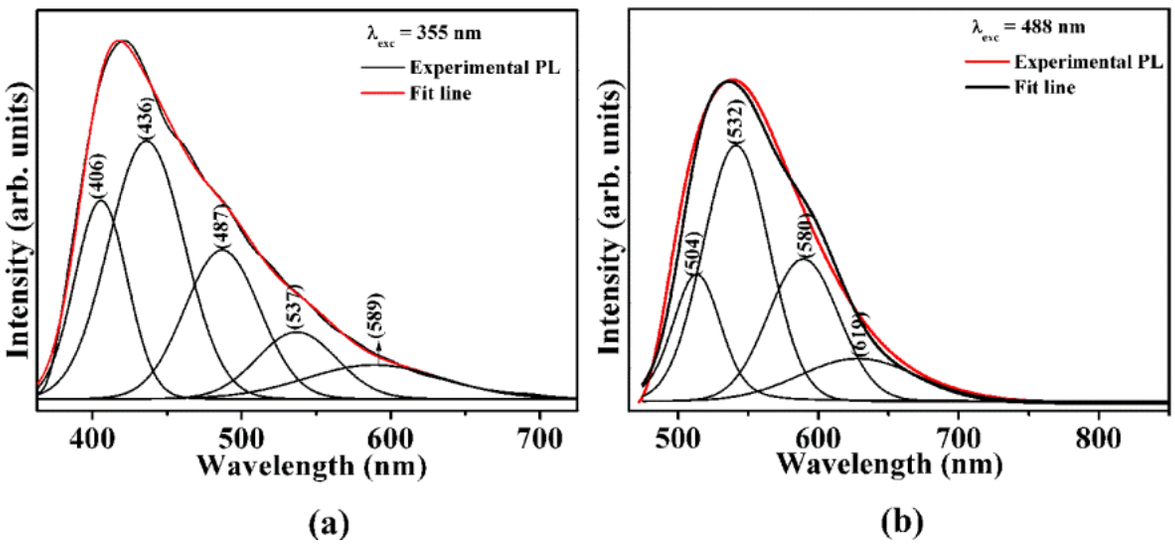

Figure 10. Deconvolution of PL curve fitted for the sample annealed at 500°C: (a) excitation with 355 nm wavelength and (b) excitation with 488 nm wavelength.

BCT20 annealed at 500°C					
Peak center (nm)					
λ (nm)	599	537	487	436	406
355 nm	%a	%a	%a	%a	%a
	9	10	22	38	20
Peak center (nm)					
λ (nm)	619	580	532	504	
488 nm	%a	%a	%a	%a	
	17	27	45	11	
599 nm= orange component of PL; 580 = yellow component of PL; 532 and 537 nm = green component of PL; 487 nm = blue component; 436 and 406 = violet component of PL. % [a] obtained by dividing the area of each decomposed PL curves by the total PL area.					

Table 1. Fitting parameters of Gaussian peaks.

X-ray Absorption Near Edge Structure (XANES) experimental results [42] pointed that the oxygen vacancies in titanates can occur in three different charge states: the [TiO_5. V_0^x] complex states, which is neutral relative and presents two electrons paired, the singly ionized [TiO_5. $V_0^\bullet$] complex state, that has one electron despaired, and the doubly positively charged [TiO_5. $V_0^{\bullet\bullet}$] complex state, which did not trap any electrons. Before donor excitation, a hole in the acceptor and an electron in a donor are created, according according to equations (2-4) using Kröger-Vink notation [43]:

$$\left[TiO_6\right]_x + [TiO_5.V_O^x] \rightarrow \left[TiO_6\right]' + [TiO_5.V_O^\bullet] \quad (4)$$

$$\left[TiO_6\right]_x + [TiO_5.V_O^\bullet] \rightarrow \left[TiO_6\right]' + [TiO_5.V_O^{\bullet\bullet}] \quad (5)$$

$$[TiO_5.V_O^{\bullet\bullet}] + 1/2\left(O_2\right) \rightarrow \left[TiO_6\right] \quad (6)$$

where [TiO_6]′ is donor, [TiO_5. $V_O^\bullet$] is donors-acceptor and [TiO_5. $V_O^{\bullet\bullet}$] is acceptor.

These equations suggest that to the transition of a valence-band hole in the conduction band is a necessary requirement the oxygen-vacancy-trapped electron in the valence band. This means that most of electrons around oxygen vacancies are released and, therefore, such oxygen vacancy complex site is relatively positive charged. Moreover, oxygen vacancies tend to trap photo-generated electrons. The charge transfer occurring as proposed in the equations (2-4) create electrons and hole polarons that can be designed as bipolarons. After the photon excitation, the recombination and decay process follow the many valid hypotheses presented in the literature [44]. The present work shows that the emission process leading to PL is facilitated by previous existence of these complex clusters in the ground state. The order-disorder BCT20 powders thus intrinsically possess the necessary condition for creating PL at room temperature.

4. Conclusion

$Ba_{0.8}Ca_{0.2}TiO_3$ (BCT) compounds prepared by Complex Polymerization Method (CPM) showed effective chelation processes of the Ba-Ca-Ti-CA in initial precursor. The CPM shown is one advantageous method because in your simple procedure is used lower temperature and smaller reaction time. The other advantage of CPM is the low cost for the production of BCT powders.

The ordering system at short and long range was accompanied for the $Ba_{0.8}Ca_{0.2}TiO_3$ using Raman, PL band and XRD characterization. Raman data related to short-range and XRD results at long-range order shows that the material is organized at 600°C. However, the phenomenon of PL at room temperature is not observed in the order structure at 600°C. The introduction of Ca^{2+} ion in $BaTiO_3$ proportioned intrinsic defects. These intrinsic defects, linked to structural disorder, facilitate the main emission process to PL. Disorder in solids

provokes degeneracy and destabilization in the localized states of the atoms acting as electron-hole pairs and supporting the broad PL band phenomena and electronic levels are fundamental to understanding the order-disorder process in the solid state. These optical properties exhibited by disordered BCT20 suggest that this material is a highly promising candidate for photoluminescent applications.

Author details

Fabiana V. Motta*, Carlos A. Paskocimas, Mauricio R. D. Bomio and Amélia S. F. Santos
Department of Materials Engineering, Federal University of Rio Grande do Norte, UFRN, Natal, RN, Brazil

Ana Paula A. Marques
Department of Exact and Earth Sciences, Federal University of São Paulo, UNIFESP, São Paulo, SP, Brazil

Edson R. Leite
Interdisciplinary Laboratory of Electrochemistry and Ceramics, Department of Chemistry, Federal University of São Carlos, UFSCar, São Carlos, SP, Brazil

José A. Varela and Elson Longo
Interdisciplinary Laboratory of Electrochemistry and Ceramics, Chemistry Institute, São Paulo State University, UNESP, Araraquara, SP, Brazil

Acknowledgement

This work was supported by Rede de Pesquisa em Catalisadores Ambientais – RECAM (grant no 564913/2010-3/CNPq) and FAPESP-CEPID (grant no 98/14324-8).

5. References

[1] Kakihana M., Yoshimura, M. (1999) Synthesis and Characteristics of Complex Multicomponent Oxides Prepared by Polymer Complex Method. Bull.Chem.Soc.Jpn 72:(1427-1443.

[2] Cho, W. S. (1998) Structural evolution and characterization of $BaTiO_3$ nanoparticles synthesized from polymeric precursor. J. Phys. Chem. Solids 59:(5) 659-666.

[3] Maurera, M., Souza, A. G., Soledade, L. E. B., Pontes, F. M., Longo, E., Leite, E. R.Varela, J. A. (2004) Microstructural and optical characterization of $CaWO_4$ and $SrWO_4$ thin films prepared by a chemical solution method. Mater. Lett. 58:(5) 727-732.

[4] Kakihana, M., Arima, M., Nakamura, Y., Yashima, M.Yoshimura, M. (1999) Spectroscopic characterization of precursors used in the Pechini-type polymerizable complex processing of barium titanate. Chem. Mat. 11:(2) 438-450.

* Corresponding Author

[5] Leite, E. R., Paris, E. C., Pontes, F. M., Paskocimas, C. A., Longo, E., Sensato, F., Pinheiro, C. D., Varela, J. A., Pizani, S. S., Campos, C. E. M. Lanciotti, F. (2003) The origin of photoluminescence in amorphous lead titanate. J. Mater. Sci. 38:1175-1179.

[6] Pontes, F. M. (2004) Characterization of $BaTi_{1-x}Zr_xO_3$ thin films obtained by a soft chemical spin-coating technique. J. Appl. Phys. 96:(8) 4386-4391.

[7] Pontes, F. M. (2003) Theoretical and experimental study on the photoluminescence in BaTiO3 amorphous thin films prepared by the chemical route. J. Lumin 104:(3) 175-185.

[8] Marques, A. P. D., de Melo, D. M. A., Paskocimas, C. A., Pizani, P. S., Joya, M. R., Leite, E. R. Longo, E. (2006) Photoluminescent $BaMoO_4$ nanopowders prepared by complex polymerization method (CPM). J. Solid State Chem. 179:(3) 671-678.

[9] Marques, A. P. A., de Melo, D. M. A., Longo, E., Paskocimas, C. A., Pizani, P. S.Leite, E. R. (2005) Photoluminescence properties of $BaMoO_4$ amorphous thin films. J. Solid State Chem. 178:(7) 2346-2353.

[10] de Figueiredo, A. T., Longo, V. M., de Lazaro, S., Mastelaro, V. R., De Vicente, F. S., Hernandes, A. C., Siu Li, M., Varela, J. A.Longo, E. (2007) Blue-green and red photoluminescence in $CaTiO_3$:Sm. J. Lumin. 126:(2) 403-407.

[11] Zhang, Q. S., Cagin, T.Goddard, W. A. (2006) The ferroelectric and cubic phases in $BaTiO_3$ ferroelectrics are also antiferroelectric. Proc. Natl. Acad. Sci. U. S. A. 103:(40) 14695-14700.

[12] Ahadi, K., Mahdavi, S.-M., Nemati, A., Tabesh, M.Ranjbar, M. Electronic structure and morphological study of BaTiO3 film grown by pulsed-laser deposition. Mater. Lett. 72:107-109.

[13] Takahashi, H. Development of lead-free $BaTiO_3$ ceramics possessing enhanced piezoelectric properties. Elect. Comm. Jp 95:(4) 20-26.

[14] Sonia, Patel, R. K., Kumar, P., Prakash, C.Agrawal, D. K. Low temperature synthesis and dielectric, ferroelectric and piezoelectric study of microwave sintered $BaTiO_3$ ceramics. Ceram. Int. 38:(2) 1585-1589.

[15] Duan, Y., Tang, G., Chen, C., Lu, T.Wu, Z. First-principles investigations of ferroelectricity and piezoelectricity in $BaTiO_3/PbTiO_3$ superlattices. Phys. Rev. B 85:(5)

[16] Motta, F. V., Marques, A. P. A., Espinosa, J. W. M., Pizani, P. S., Longo, E.Varela, J. A. (2010) Room temperature photoluminescence of BCT prepared by Complex Polymerization Method. Curr. Appl. Phys. 10:(1) 16-20.

[17] Kumar, P., Singh, S., Juneja, J. K., Prakash, C.Raina, K. K. Influence of calcium substitution on structural and electrical properties of substituted barium titanate. Ceram. Int. 37:(5) 1697-1700.

[18] Sonia, Patel, R. K., Prakash, C.Kumar, P. Effect of microwave processing on structural, dielectric and ferroelectric properties of calcium-doped $BaTiO_3$ ceramics. J. Ceram. Process. Res. 12:(6) 634-639.

[19] Chen, X. M., Wang, I.Li, J. (2004) Dielectric characteristics and their field dependence of (Ba, Ca)TiO_3 ceramics. Mater. Sci. Eng. B-Solid State Mater. Adv. Technol. 113:(2) 117-120.

[20] Chang, M. C.Yu, S. C. (2000) Raman study for $(Ba_{1-x}Ca_x)TiO_3$ and $Ba(Ti_{1-y}Ca_y)O_3$ crystalline ceramics. J. Mater. Sci. Lett. 19:(15) 1323-1325.

[21] Suzuki, T., Ueno, M., Nishi, Y. Fujimoto, M. (2001) Dislocation loop formation in nonstoichiometric (Ba,Ca)TiO_3 and $BaTiO_3$ ceramics. J. Am. Ceram. Soc. 84:(1) 200-206.
[22] Kuper, C., Pankrath, R.Hesse, H. (1997) Growth and dielectric properties of congruently melting $Ba_{1-x}Ca_xTiO_3$ crystals. Appl. Phys. A-Mater. Sci. Process. 65:(3) 301-305.
[23] Cheng, X.Shen, M. (2007) Different microstructure and dielectric properties of Ba1-xCaxTiO3 ceramics and pulsed-laser-ablated films. Materials Research Bulletin 42:(1662.
[24] Pontes, F. M., Longo, E., Leite, E. R., Lee, E. J. H., Varela, J. A., Pizani, P. S., Campos, C. E. M., Lanciotti, F., Mastelaro, V.Pinheiro, C. D. (2003) Photoluminescence at room temperature in amorphous $SrTiO_3$ thin films obtained by chemical solution deposition. Mater. Chem. Phys. 77:(2) 598-602.
[25] Orhan, E., Varela, J. A., Zenatti, A., Gurgel, M. F. C., Pontes, F. M., Leite, E. R., Longo, E., Pizani, P. S., Beltran, A. Andres, J. (2005) Room-temperature photoluminescence of BaTiO3: Joint experimental and theoretical study. Phys. Rev. B 71:(8) 085113.
[26] Motta, F. V., de Figueiredo, A. T., Longo, V. M., Mastelaro, V. R., Freitas, A. Z., Gomes, L., Vieira, N. D., Jr., Longo, E. Varela, J. A. (2009) Disorder-dependent photoluminescence in $Ba_{0.8}Ca_{0.2}TiO_3$ at room temperature. J. Lumin. 129:(7) 686-690.
[27] Pizani, P. S., Leite, E. R., Pontes, F. M., Paris, E. C., Rangel, J. H., Lee, E. J. H., Longo, E., Delega, P. Varela, J. A. (2000) Photoluminescence of disordered ABO_3 perovskites. Appl. Phys. Lett. 77:(6) 824-826.
[28] Pizani, P. S., Basso, H. C., Lanciotti, F., Boschi, T. M., Pontes, F. M., Longo, E. Leite, E. R. (2002) Visible photoluminescence in amorphous ABO_3 perovskites. Appl. Phys. Lett. 81:(2) 253-255.
[29] Orhan, E., Albarici, V. C., Escote, M. T., Machado, M. A. C., Pizani, P. S., Leite, E. R., Sambrano, J. R., Varela, J. A. Longo, E. (2004) A DFT rationalization of the room temperature photoluminescence of Li_2TiSiO_5. Chem. Phys. Lett. 398:(4-6) 330-335.
[30] Longo, V. M., Cavalcante, L. S., de Figueiredo, A. T., Santos, L. P. S., Longo, E., Varela, J. A., Sambrano, J. R., Paskocimas, C. A., De Vicente, F. S. Hernandes, A. C. (2007) Highly intense violet-blue light emission at room temperature in structurally disordered $SrZrO_3$ powders. Appl. Phys. Lett. 90:(9) 091906.
[31] Rajendran, M.Rao, M. S. (1994) Formation of $BaTiO_3$ from Citrate Precursor. J. Solid State Chem. 113:(2) 239-247.
[32] Yasodhai, S., Sivakumar, T.Govindarajan, S. (1999) Preparation, characterisation and thermal reactivity of transition metal complexes of hydrazine with citric acid. Thermochim. Acta 338:(1-2) 57-65.
[33] Fang, T. T. Tsay, J. D. (2001) Effect of pH on the chemistry of the barium titanium citrate gel and its thermal decomposition behavior. J. Am. Ceram. Soc. 84:(11) 2475-2478.
[34] Duran, P., Gutierrez, D., Tartaj, J., Banares, M. A. Moure, C. (2002) On the formation of an oxycarbonate intermediate phase in the synthesis of BaTO3 from (Ba,Ti)-polymeric organic precursors. J. European Ceram. Soc. 22:(6) 797-807.
[35] Deng, Y. F., Zhou, Z. H. Wan, H. L. (2004) pH-dependent isolations and spectroscopic, structural, and thermal studies of titanium citrate complexes. Inorg. Chem. 43:(20) 6266-6273.

[36] Kumar, S. Messing, G. L. (1994) Metal-Organic Resin Derived Barium-Titanate .2. Kinetics of $BaTiO_3$ Formation. J. Am. Ceram. Soc. 77:(11) 2940-2948.

[37] Kumar, S., Messing, G. L.White, W. B. (1993) Metal-Organic Resin Derived Barium-Titanate .1. Formation of Barium Titanium Oxycarbonate Intermediate. J. Am. Ceram. Soc. 76:(3) 617-624.

[38] Duran, P., Capel, F., Tartaj, J., Gutierrez, D. Moure, C. (2001) Heating-rate effect on the BaTiO3 formation by thermal decomposition of metal citrate polymeric precursors. Solid State Ion. 141:(529-539.

[39] Street, R. A. (1976) Luminescence in Amorphous-Semiconductors. Adv. Phys. 25:(4) 397-453.

[40] Ding, T., Zheng, W. T., Tian, H. W., Zang, J. F., Zhao, Z. D., Yu, S. S., Li, X. T., Meng, F. L., Wang, Y. M.Kong, X. G. (2004) Temperature-dependent photoluminescence in $La_{2/3}Ca_{1/3}MnO_3$. Sol. St. Commun. 132:(12) 815-819.

[41] Gurgel, M. F. C., Espinosa, J. W. M., Campos, A. B., Rosa, I. L. V., Joya, M. R., Souza, A. G., Zaghete, M. A., Pizani, P. S., Leite, E. R., Varela, J. A. Longo, E. (2007) Photoluminescence of crystalline and disordered BTO : Mn powder: Experimental and theoretical modeling. J. Lumin. 126:(2) 771-778.

[42] Asokan, K., Jan, J. C., Chiou, J. W., Pong, W. F., Tseng, P. K. Lin, I. N. (2001) X-ray absorption spectroscopy studies of $Ba_{1-x}Ca_xTiO_3$. J. Synchrot. Radiat. 8: 839-841.

[43] Kröger, F. A., Vink, H. J. Frederick Seitz, David, T. (1956). Relations between the Concentrations of Imperfections in Crystalline Solids, Vol. 3, Sol. St. Phys. 3: 307-435. Academic Press.

[44] Leonelli, R. Brebner, J. L. (1986) Time-Resolved Spectroscopy of the Visible Emission Band in Strontium-Titanate. Phys Rev B. 33:8649-8656.